journal

J. Am. Ceram. Soc., 96 [1] 96–102 (2013)
DOI: 10.1111/jace.12078

Size and Shape Tailoring of Titania Nanoparticles Synthesized by Solvothermal Route in Different Solvents

Roman Alvarez Roca† and Edson Roberto Leite†

Department of Material Science and Engineering and Chemistry Department, Federal University of Sao Carlos, Sao Carlos, SP 13656-905, Brazil

A simple solvothermal low-temperature synthesis process of TiO_2 nanoparticles was investigated in different solvents [Octanol (Oc), Ethanolamine (Am) and Terathane (Tr)] with titanium (IV) chloride ($TiCl_4$) as precursor. The samples were characterized by X-Ray Diffraction (XRD) and Transmission Electron Microscopy (TEM). XRD showed the crystallite size ranging from 4 to 12 nm, which were calculated using Debye–Scherrer's equation. The existence of poor or high crystalline anatase phases and high crystalline anatase/rutile mixture was also shown. TEM images displayed variations in the morphological behavior depending on the synthesis condition. Particles of irregular morphology with high irregular agglomeration up to well-defined particles can be observed, which are self-assembled by oriented attachment (OA). This self-assembly led to TiO_2 microparticles with 3-D Wulff shape for anatase and 1-D shape for rutile. The results showed that the TiO_2 nanopowder could be easily engineered and adapted by the solvent type, the $TiCl_4$ concentration and the synthesis time.

I. Introduction

The synthesis of titanium oxide (TiO_2) nanomaterials has been intensively studied due to their particularly attractive chemical and physical properties, which are of interest to applications in sensing, photochemical water splitting, photocatalysis, photovoltaics, and dye-sensitized solar cells.[1–5] Depending on the application, a wide variety of requirements must be fulfilled, such as particle size, shape, crystal structure, and phase composition. In addition to the TiO_2 nanoparticle synthesis with these controlled requirements, the fabrication and use of one-, two-, and three-dimensional superstructures from nanoparticles as building blocks has attracted much attention.[6–10] This multidimensional architecture may exhibit interesting properties combining nano-micro scales with the anisotropic character.

Over the last years, a well-established mechanism for the growth of multidimensional TiO_2 is the oriented attachment (OA) mechanism.[11–15] In this process, low mass and very large surface area nanocrystallites can cluster spontaneously to reduce overall energy by removing surface energy, attracted by adjacent exposed surfaces with a common crystallographic orientation. The OA mechanism is relevant in cases where particles are free to move, which can take place in a well dispersed or a weakly flocculated colloidal state.[13]

Due to of the importance of TiO_2 nanoparticles, the extensive advance in the nanotitania synthesis approach is not surprising. Among these, nonaqueous processes, as nonaqueous sol-gel and solvothermal, have shown to be versatile synthesis procedures.[1,11,16,17] The nonaqueous routes offer the possibility to use different organic solvents in the reaction, hence, to explore a large variety of parameters (molecular weight, polarity, solubility, active groups, etc.) and their influence on the reaction pathways and the final products.[11,16,17] This large range of experimental conditions allows a better choosing, controlling, and understanding the reaction at the molecular level.

The effects of different organic compounds as oxygen source and for controlling shape, composition and crystal structure on the synthesis of oxide nanoparticle are reported in the reference section.[11] In particular, for TiO_2, the parameters determining the formation of either anatase or rutile, with varieties in the particle morphology and the solvent dependence, have been investigated in several works.[11,18]

In previous works, we described the synthesis of TiO_2 nanoparticles using the nonaqueous process.[14,19] In fact, we describe a kinetically controlled crystallization process assisted by an OA mechanism based on the reaction of titanium (IV) chloride ($TiCl_4$) with different solvents to prepare recrystallized anatase TiO_2 mesocrystals. The kinetics study revealed a multistep and hierarchical process controlled by OA, and a high-resolution transmission electron microscopy (HRTEM) analysis clearly shows that the synthesized mesocrystal presents a truncated bipyramidal Wulff shape, indicating that its surface is dominated by {101} facets.[14]

In this study, we focused on the solvothermal synthesis of TiO_2 nanoparticles and their phase composition and microstructure behaviors. First, we studied the formation and growth of TiO_2 particles synthesized using $TiCl_4$ as a precursor in three different solvents. The influence of the synthesis time, as well as the precursor concentration on the crystallinity degree, crystallite size, phase composition, and anatase–rutile transformation were analyzed. Second, we explored the nanoparticle self-organization on secondary particles or structures by an OA mechanism which results in a hierarchical growth process. The results confirmed that this is a good method to prepare TiO_2 nanopowder and that OA is an important mechanism in these systems.

II. Experimental Procedure

Titanium(IV) chloride ($TiCl_4$, 99.99%), n-Octanol (Oc) ($CH_3(CH_2)_7OH$, 99%), 2-Ethanolamine (Am) (NH_2CH_2-CH_2OH, $\geq$99.0%), and polytetramethylene ether glycol ($(C_4H_8O)_n(OH)_2$, 99.9%) –Terathane (Tr), average molecular weight M_w = 1000 g/mol were purchased from Sigma-Aldrich. All chemicals were used without further purification.

The synthesis was conducted in a dry box under controlled atmosphere. In a glove box, $TiCl_4$ was added to the solvent. Three different solvents were used: n-Octanol, 2-Ethanolamine, and Terathane 1000. Solutions with different $TiCl_4$: solvent molar ratios were prepared (1:10, 5:10, and 10:10). The reaction vessel was removed from the glove box and heated in the silicone oil bath. The temperature was

P. Gouma—contributing editor

Manuscript No. 31669. Received July 3, 2012; approved October 12, 2012.
†Authors to whom correspondence should be addressed. e-mails: cortes116@yahoo.es and edson.leite@pq.cnpq.br

controlled at 120°C and with different synthesis times that ranged from 24 to 72 h. A precipitated white powder was washed several times with absolute ethanol, the remaining liquid was removed by centrifugation and was then dried overnight at 60°C.

X-Ray Diffraction (XRD) analysis (Cu$K\alpha$, λ = 1.54056 Å) was performed using a Rigaku D/MAX-2500 diffractometer (Rigaku Corporation, Tokyo, Japan). The scanning step size was 0.02 in 2θ with a counting time of 1 s per step. Transmission electron microscopy (TEM) was performed with a TECNAI F20 FEI microscope (FEI Company, Eindhoven, the Netherlands) operated at 200 kV. Other supplementary analyses were performed. The specific surface area and mass loss, by Thermogravimetric Analysis (TGA), were measured using a BET surface area analyzer, Micrometrics/ASAP 2000 (Micromeritrics, Norcross, GA), and a Netzsch STA 409 (Netzsch Company, Selb, Germany) model, respectively.

III. Results and Discussion

Figure 1 depicts the X-ray diffraction (XRD) pattern of the as-synthesized products with different solvents. Figure 1(a) shows, for Am, Tr, and Oc synthesized with low $TiCl_4$ concentration, 1:10 molar ratio. The data confirmed that all products were tetragonal-structured anatase TiO_2 and no characteristic peaks of other phases were detected. The diffraction peaks are broad due to the small particle size. For Tr and Oc, the (101) peak of anatase is sharp, indicating an intensive growth process for the crystalline nanoparticles. Note that for Tr, in addition to the main crystalline peak, a characteristic hump is observed, not very intense, which can be an amorphous background from a low relative percentage of uncrystallized powder. For Am, the very broad and low intensity (101) peak can be the result of the poorly crystallized powder (great amount of amorphous material) and small-sized crystallite particles. With further increase in the $TiCl_4$ concentration, 5:10 and 10:10 molar ratio, in Fig. 1(b); the shapes of the powders synthesized in Am and Tr displayed slight variations in relation to the low concentration. Interestingly, the peaks corresponding to rutile TiO_2 become more apparent when the solvent is Oc.

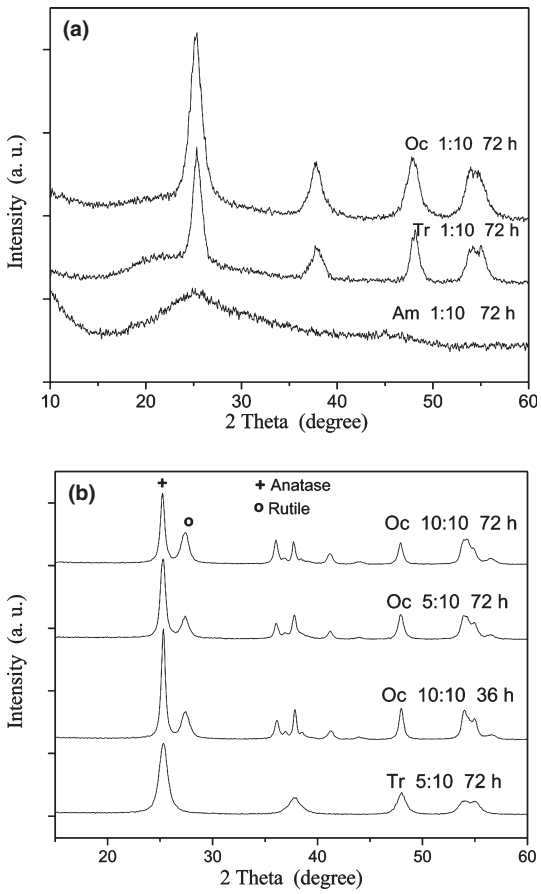

Fig. 1. XRD patterns of TiO_2 nanoparticles prepared at different reaction conditions: (a) 1:10 molar ratio (low $TiCl_4$ concentration) and 72 h for the three different solvents and (b) for Tr and Oc at higher molar ratio, 5:10 and 10:10, and synthesis times, 36 and 72 h. The more intense peak for Anatase and Rutile phase are shown.

Crystallite sizes for anatase, D_a, and rutile, D_r, were estimated from the Debye–Scherrer formula[20] using the (101) peak and the (110) peak of anatase and rutile, respectively. The composition of the relative phase of anatase and rutile was also calculated from the integrated intensities of the above-mentioned peaks. The rutile fraction is calculated using the following equation:

$$\%\,\text{transformation of rutile}(W_R) = \frac{1}{\left(1 + 0.8\left(\frac{I_A}{I_R}\right)\right)} \qquad (1)$$

where I_A and I_R are the integrated intensity of anatase and rutile, respectively (the integrated intensity was calculated after the instrumental broadening was corrected).

Table I shows the results for average size and percentage transformation of rutile. For Am and Oc, with low $TiCl_4$ concentration, the smaller particle sizes were synthesized. When the $TiCl_4$ concentration and synthesis time were increased, the particle size slightly increases for the synthesis in Tr, without evidence of the rutile phase. However, when Oc is used as solvent, concentration and time effects on particle size and rutile fraction were more pronounced.

TEM characterization of the as-prepared powder for low $TiCl_4$ concentration exhibited small particles, 3–5 nm in size, for all solvents; in reasonable agreement with the XRD observations; see Table I. All images in Fig. 2 show that the powders are composed of nanoparticles with the formation of a larger number of agglomerates. Figure 2(a) shows a great amount of amorphous material when Am is the solvent, this poor crystallization state is in good agreement with the XRD results. The TiO_2 morphology consisted of irregular nanoparticles and misorientation at the interparticle connections, which were the predominant facts when using Am and Tr as solvent, as seen in Figs. 2(a) and (b). However, the synthesis in Oc, Fig. 2(c), exhibited particles with a more uniform morphology, truncated tetragonal bipyramidal shape, accompanied by the increase in events with OA.

When the $TiCl_4$ concentration is increased, 5:10 molar ratio, in the reaction with Am, no significant changes in the crystallinity degree of the powder were observed (not shown here). Moreover, an appreciable amount of amorphous material persists in the final product. Several approaches to TiO_2 synthesis by nonaqueous process at room temperature in the amine system as solvent are reported in the literature. Jung

Table I. Crystallite Size and Phase Contents, Anatase and Rutile, of Titania Products Synthesized for Various Molar Ratios and Reaction Times

Solvent	Molar ratio ($TiCl_4$:Solvent)	Synthesis time (h)	D_a (nm)	D_r (nm)	% Rutile
Am	1:10	72	3.90	–	–
Tr	1:10	72	4.98	–	–
	5:10	36	6.00	–	–
	5:10	72	7.64	–	–
	10:10	72	8.46	†	†
Oc	1:10	72	5.14	–	–
	5:10	36	6.03	†	†
	5:10	72	13.78	8.88	27.51
	10:10	36	17.96	8.90	24.72
	10:10	72	16.56	10.10	36.00

†Undetected by XRD

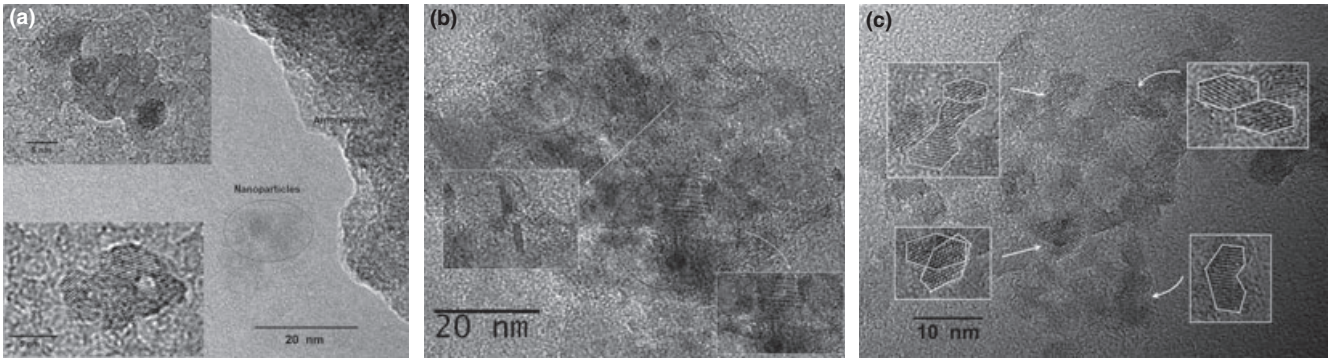

Fig. 2. TEM images of TiO_2 nanoparticles with 1:10 molar ratio (low $TiCl_4$ concentration). Details of the amorphous phase, nanoparticle clusters with partially or complete OA and morphology are shown for (a) Am, (b) Tr and (c) Oc. The bar of the insets in (a) is 5 nm.

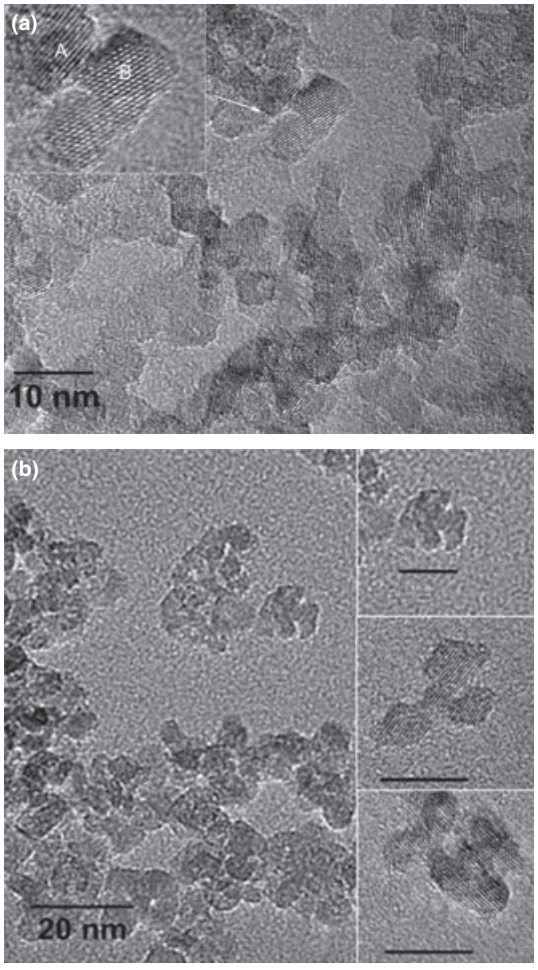

Fig. 3. TEM images of the TiO_2 nanoparticles synthesized in Tr with 5:10 molar ratio for (a) 36 h and (b) 72. Inset in (a) and (b) show partial and complete OA between the particles; in (b) the bar in insets is 10 nm.

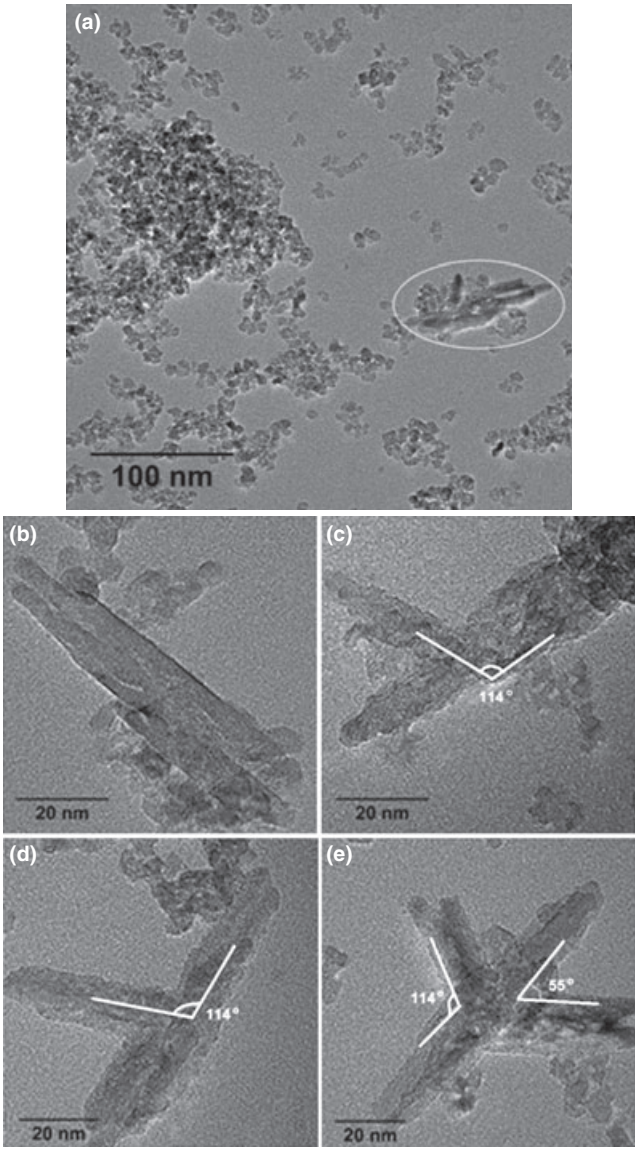

Fig. 4. TEM images for TiO_2 nanoparticles synthesized in Tr with 10:10 molar ratio at 72 h. The circle in (a) shows a branched structure. (b) The individual nanorods structure and (c)–(e) the branched nanorod structure.

et al.[21] on Am and Valverde-Aguilar *et al.*[22] on Diethanolamine reported the synthesis of amorphous TiO_2 as final product. Liu and co-worker[23] have also reported the amorphous TiO_2 synthesis in Diethanolamine with high mass loss (~70%) during thermal treatment. We found a mass loss of 52% in our experiments, the greatest of all the solvents used. Increases in synthesis temperature and alkyl length of amine result in more crystalline nanoparticles. However, at present, the formation mechanism and role of the active group in surface stability and crystallization state is not yet clear.

However, more interesting and diverse results are exhibited when the Tr or Oc are used in the reaction. Figure 3 shows a TEM image of the product obtained for the reaction in Tr at 5:10 molar ratio. The samples synthesized for 36 h, Fig. 3(a), and 72 h, Fig. 3(b), showed a common fact: the formation of large scale agglomerates without well-defined architecture by the self-assembly. However, with increasing time, the agglomeration degree decreased and the organization by OA was

more expanded in the particles. With a new increasing of the $TiCl_4$ concentration, 10:10 molar ratio, a better definition of the nanoparticle morphology was obtained. Particularly, the synthesis at 72 h, Fig. 4, shows that in addition to anatase nanoparticle population, a few nanorod structures are observed. Such 1-D structures (nanorods, nanowire, etc.) are commonly assigned to the rutile phase. The low observation frequency of this nanorod structure in the sample is consistent with the non detected rutile phase by XRD. Besides, the individual nanorod structure, Fig. 4(b), minor branched structures can also be found, marked by a circle in Fig. 4(a). Figures 4(b)–(e) shows the TEM image magnification of these structures, individual nanorods, and branched nanorods. The nanorod structures have a length that ranges between 60 and 90 nm for the individual or central arm, in the nanorod branches, and 25 and 40 nm for the lateral arm. For the branched structures, two kinds of angles can be observed, 114° [Figs. 4(c)–(e)] and 55° [Fig. 4(e)]. The synthesis of rutile TiO2 multibranched structures has been reported in several works.[9,10,15,24–26] Some of these works reported that the variations in branch morphology are due to the fact that there are two types of twin boundaries, which result in the two types of angles: the most common (101) twin, in agreement with our observations, and the less common (301) twin for 114° and 55°, respectively.

Experiments with same molar ratios, 5:10 and 10:10, and 36–72 h synthesis times were carried out with Oc as solvent. The TEM images of the samples obtained at different reaction conditions are shown in Fig. 5. Under such experimental conditions, the formation of large secondary particles with well-defined architecture was observed. The images show similar morphological behavior according to[14] on Oc for synthesis at 100°C. The nanopowders are mainly composed by truncated bipyramidal Wulff structures as secondary particles with a rough surface. These secondary particles are made up of many packed nanocrystallites with a bipyramidal morphology assembly by OA. The incomplete formation of Wulff structures is also observed in some secondary particles and their relatively broad size distribution can be evidences of a hierarchical growth process during the self-assembly, as suggested in.[14]

To confirm the Wullf structure phase, we also examined the nanomaterials by HRTEM. Figure 6(a) is the corresponding HRTEM image of two alternative geometries for the bi-dimensional projection of the truncated tetragonal bipyramidal Wulff shape in two different zone axes. They showed clear lattice fringes, which allow to identify the crystallographic spacing. Some detailed characteristics (lattice spacing of crystallographic plane, zone axes, Fast Fourier Transform, angle between planes) are displayed in Fig. 6(b), which confirm the anatase structure.

As shown in the TEM image in Fig. 5, large nanowires of several sizes coexist in the samples, which could be related to the rutile phase detected by XRD. This wide size range and the agglomeration degree make difficult to determine the average length to study the effects of increasing $TiCl_4$ concentration and synthesis time on the nanowire dimensions. Although, with suitable approximation, it can be estimated that for 5:10 at 72 h and for 10:10 at 36 h, the particle size may range from 250 to 350 nm in length; up to >450 nm for 10:10 mol ratio at 72 h. An analysis of the lattice images in this nanowire taken by HRTEM, in Fig. 7, proves its rutile structure. The interplanar spacing of 0.32 nm is (110) the crystallographic plane of rutile, confirmed by the insert FFT pattern along the [001] zone axis.

Our group[14] reported the synthesis of anatase for the reaction of $TiCl_4$ with Oc at 100°C with traces of rutile in a concentration lower than 5%. Only the considerable formation of rutile was observed when a magnetic stirrer is used during the synthesis (see ESI for[14]). The presence of the rutile phase was related to the retention of HCl in the reaction system. As it is known, an acid environment will suppress the growth of anatase particles and will favor the formation of the rutile phase.[27–29] We suggested that, for its static system, the presence of Oc attached to the surface invalidates the interaction between HCl and the anatase particles, and this resulted in a very low rutile concentration.

In our work, increasing the $TiCl_4$ concentration and synthesis time will increase the rutile percentage because more HCl is formed in the reaction system. This confirmed the favorable effect of the acid environment on the formation of rutile. In contrast with,[14] for similar molar ratio, we obtained a higher rutile concentration. This can be attributed to a higher temperature used in our experiments. An excess of thermal energy can promote the Brownian motion, similar to the magnetic stirrer, and hence the frequency and strength of the collisions between particles is increased. These two factors can contribute to the breaking of the solvent bond with the surface and promotes the HCl–surface interaction. Another consequence of the temperature increase can be considered, such as a higher surface area to volume ratios expected for the nanoscale grains increasing the total surface energy. Therefore, from an energetic point of view, less energy is required to activate the phase transformation and relatively little increases in temperature can supply sufficient energy to increase the transformation rate.

Thus, an illustrative study of the phase transformation kinetics was carried out. This kinetics study is based on previous work[14] and presents experimental results for rutile weight fraction, x, versus the synthesis time, t, and annealing temperature, T, from XRD spectra. Following the Avrami Equation[30]: $x = 1-\exp(kt)^n$ (where k and n are the rate constant and a constant that depends on the mechanism, respectively), the plot of $\ln \ln(1-x)$ versus $\ln t$ with a regression line is fitted. The activation energy for the anatase to rutile transformation can be determined from the slope of an Arrhenius plot of $\ln k$ versus $1/T$. The n values were calculated in the 1.1–1.2 range and the activation energy was 35 kJ/mol. This latter value is slightly higher than the previous report: 7.5–21 kJ/mol[31] and 20 kJ/mol[32] for TiO_2 nanoparticles

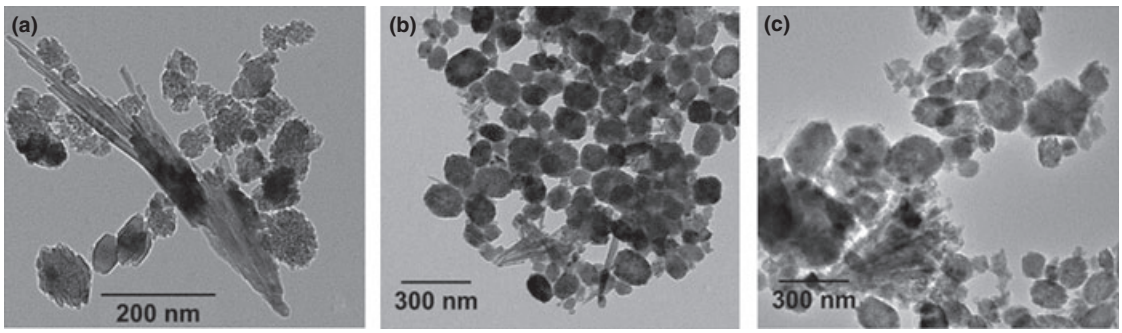

Fig. 5. TEM images of TiO_2 nanoparticles synthesized in Oc with (a) 5:10 and 72 h, (b) 10:10 and 36 h, and (c) 10:1 and 72 h molar ratio and synthesis time, respectively.

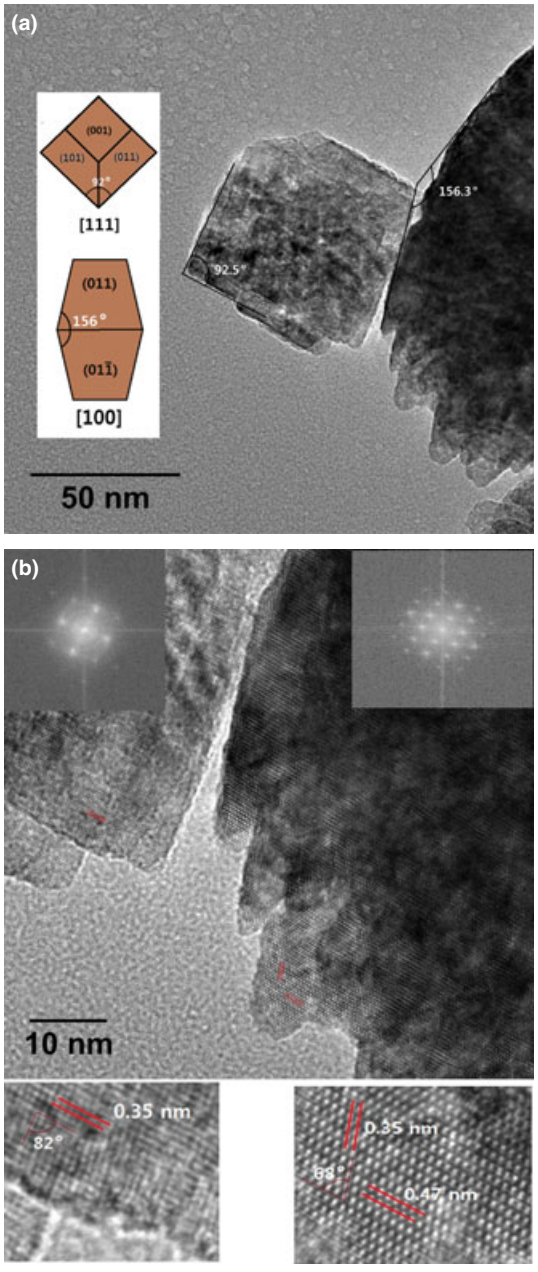

Fig. 6. HRTEM images of the TiO_2 anatase secondary nanoparticles synthesized in Oc show (a) two alternative bi-dimensional Wulff shape projection and (b) an analysis of lattice images. The lattice spacing of 0.35 nm is (101) crystallographic plane, whereas the 0.47 nm corresponds to the spacing of the (002) plane. The insert shows the Fast Fourier Transform (FFT) pattern along the [010] zone axis.

using a nonaqueous method. In addition to the high surface area, there are other factors in our system, such as the uniform shape and narrow size distribution of the nanoparticles, and the interfacial defects (typical of OA process) play an important role in the phase transition and in the low activation energy value.

Comparatively analyzing the solvent effects, of Tr and Oc, on the phase composition and morphology, some interesting differences were observed. The rutile percentage and OA extension, which can be associated with the phase transformation rate and the surface characteristics, respectively, are the most emphasized ones. We explain these different behaviors mainly based on the different chain lengths of the solvents.

As shown, the rutile phase concentration increases with the molar ratio and, correspondingly, with $TiCl_4$ concentration. This concentration effect can be attributed to the acidity (HCl) variation. In other words, high concentration results in high acidity, which favors the formation of the rutile phase. However, with a similar molar ratio, a much lower rutile content is detected in the reaction when Tr is used as solvent, when compared with Oc. Therefore, the acid environment is not considered a sufficient condition and the effectiveness of the interaction between surface and HCl can be considered. The higher protecting ability of the Tr layer on the anatase surface, due to the higher chain length, is a limiting factor for an effective HCl–surface interaction. Similar to the results for static and dynamic (magnetic stirrer) conditions at the same concentration reported in.[14] Ding *et al.*[9] reported that the branched rutile structures became the main morphology with the decreasing Ti precursor ($TiCl_4$) concentration. In our experiments, the branched structures observed in Tr, and not in Oc for similar $TiCl_4$ concentration, are more related with this lower HCl–surface interaction. Besides the HCl–surface interaction, another effect related to the chain length should be considered: the aggregation degree of the nanoparticles and convenience for the OA. The lower chain length, for the Oc, enhanced the aggregation of the anatase nanoparticles in more dense and organized (by OA) structures. This reduces the total surface energy which facilitates the rutile nucleation.

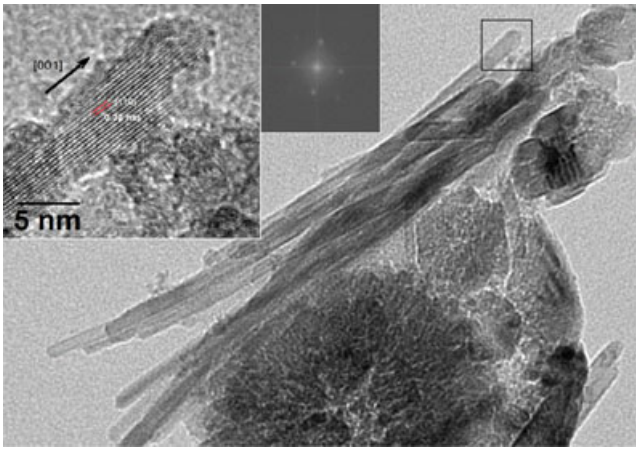

Fig. 7. HRTEM images of rutile nanowire synthesized in Oc. The inset shows high magnification and typical FFT.

On the other hand, the results observed in this study strongly support the evolution of the units according to the hierarchical growth mechanism. The hierarchical growth process has been reported by other authors in TiO_2 synthesis with different morphologies.[4,5,15,33,34] To understand this formation process, we assumed that our reaction system is highly inhomogeneous, compounded by an assembly of homogeneous subregions which display variations in their reaction conditions. This inhomogeneity condition may be due to the static condition (without stirrer) used in our experiments. For each one of these subregions, the nucleation and growth of nanoparticles can be described by the LaMer model.[35] Although the mechanism of the nanoparticles formation is more complex, the simpler LaMer model is used as a qualitative model to describe this phenomena. According to the model, the formation of colloidal particles is achieved by the burst nucleation process from a supersaturated solution, followed by the growth process which is controlled by either diffusion or surface reaction.

The variations in the reaction condition (environment acidity, dispersion degree, supersaturation level, etc.) lead to differences in the LaMer diagram for each subregion. The reaction kinetics and development of nanounits evolve with differences the subregion-to-subregion. Joined with this formation process, the spontaneous self-organization by AO occurs and at the end a hierarchical arrangement is

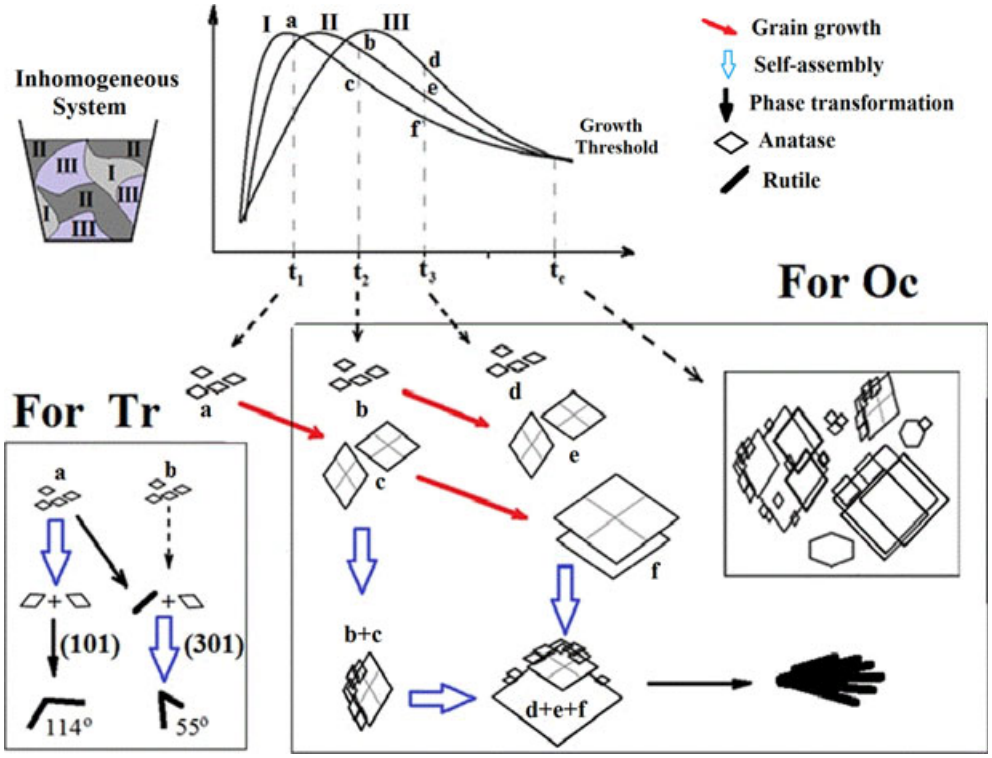

Fig. 8. Schematic presentation of LaMer model assuming an inhomogeneous system shows the time evolution for the overall reaction and the final particles morphology (with hierarchical growth), broad size distribution, and phases.

displayed. The LaMer's mechanism is depicted schematically in Fig. 8. According to this figure, for both, Tr and Oc solvent, the inhomogeneous characteristic of the reaction enables to describe the experimental facts observed. The formation of rutile multipods for Tr is in accordance with the mechanism proposed by Ding *et al.*[9]

IV. Conclusion

In this study, TiO_2 nanoparticles were synthesized using the nonaqueous method with $TiCl_4$ as the precursor in three different solvents: Oc, 2-Am, and Tr. By controlling the reaction parameters, time synthesis and precursor concentrations, we demonstrate that various simple or multidimensional morphologies are possible, such as nanoparticles, aggregated nanorods and nanowire, and 3-D Wulff structures. Although the anatase form is predominantly obtained, the rutile and amorphous forms were also confirmed depending on the reaction condition. This morphology and phase behavior was explained in terms of the HCl–surface interaction due to the chain length of the solvents. The kinetics of the hierarchical growth controlled by OA is strongly affected by the inhomogeneity of the system.

Acknowledgments

We thank R. H. Gonçalves and C. J. Dalmacio for their technical assistance and discussion of the results obtained. This work has been supported by CAPES, CNPq, and FAPESP; all Brazilian agencies.

References

[1]X. Chen and S. S. Mao, "Titanium Dioxide Nanomaterials: Synthesis, Properties, Modifications and Applications," *Chem. Rev.*, **107** [7] 2891–59 (2007).

[2]T. S. Kang, A. P. Smith, B. E. Taylor, and M. F. Durstock, "Fabrication of Highly-Ordered TiO_2 Nanotube Arrays and Their Use in Dye-Sensitized Solar Cells," *Nano Lett.*, **9** [2] 601–6 (2009).

[3]F. Sauvage, D. H. Chen, P. Comte, F. Z. Huang, L. P. Heiniger, Y. B. Cheng, R. A. Caruso, and M. Graetzel, "Dye-Sensitized Solar Cells Employing a Single Film of Mesoporous TiO_2 Beads Achieve Power Conversion Efficiencies Over 10%," *ACS Nano*, **4** [8] 4420–5 (2010).

[4]L. Xiang, X. Zhao, J. Yin, and B. Fan, "Well-Organized 3D Urchin-Like Hierarchical TiO_2 Microspheres With High Photocatalytic Activity," *J. Mater. Sci.*, **47** [3] 1436–45 (2012).

[5]Y. Tang, P. Wee, Y. Lai, X. Wang, D. Gong, P. D. Kanhere, T. Lim, Z. Dong, and Z. Chen, "Hierarchical TiO_2 Nanoflakes and Nanoparticles Hybrid Structure for Improved Photocatalytic Activity," *J. Phys. Chem. C*, **116** [4] 2772–80 (2012).

[6]H. G. Yang, G. Liu, S. Z. Qiao, C. H. Sun, Y. G. Jin, S. C. Smith, J. Zou, H. M. Cheng, and G. Q. Lu, "Solvothermal Synthesis and Photoreactivity of Anatase TiO_2 Nanosheets With Dominant {001} Facets," *J. Am. Chem. Soc.*, **131** [11] 4078–83 (2009).

[7]D. H. Chen, F. Z. Huang, Y. B. Cheng, and R. A. Caruso, "Mesoporous Anatase TiO_2 Beads With High Surface Areas and Controllable Pore Sizes: A Superior Candidate for High-Performance Dye-Sensitized Solar Cells," *Adv. Mater.*, **21** [21] 2206–10 (2009).

[8]J. K. Oh, J. K. Lee, H. S. Kim, S. B. Han, and P. W. Park, "TiO_2 Branched Nanostructure Electrodes Synthesized by Seeding Method for Dye-Sensitized Solar Cells," *Chem. Mater.*, **22** [3] 1114–8 (2010).

[9]K. Ding, Z. Miao, B. Hu, G. An, Z. Sun, B. Han, and Z. Liu, "Study on the Anatase to Rutile Phase Transformation and Controlled Synthesis of Rutile Nanocrystals With the Assistance of Ionic Liquid," *Langmuir*, **26** [12] 10294–302 (2010).

[10]W. Zhou, X. Liu, J. Cui, D. Liu, J. Li, H. Jiang, J. Wang, and H. Liu, "Control Synthesis of Rutile TiO_2 Microspheres, Nanoflowers, Nanotrees and Nanobelts via Acid-Hydrothermal Method and Their Optical Properties," *CrystEngComm*, **13** [14] 4557–63 (2011).

[11]G. Garnweitner and M. Niederberger, "Organic Chemistry in Inorganic Nanomaterials Synthesis," *J. Mater. Chem.*, **18** [11] 1171–82 (2008).

[12]Q. Zhang, S. J. Liu, and S. H. Yu, "Recent Advances in Oriented Attachment Growth and Synthesis of Functional Materials: Concept, Evidence, Mechanism, and Future," *J. Mater. Chem.*, **19** [2] 191–200 (2009).

[13]C. J. Dalmaschio, C. Ribeiro, and E. R. Leite, "Impact of the Colloidal State on the Oriented Attachment Growth Mechanism," *Nanoscale*, **2** [11] 2336–45 (2010).

[14]R. Silva, R. H. Gonçalves, D. G. Stroppa, A. J. Ramirez, and E. R. Leite, "Synthesis of Recrystallized Anatase TiO_2 Mesocrystals With Wulff Shape Assisted by Oriented Attachment," *Nanoscale*, **3** [4] 1910–6 (2011).

[15]H. Wang, Y. Liu, Z. Liu, H. Xu, Y. Deng, and H. Shen, "Hierarchical Rutile TiO_2 Mesocrystals Assembled by Nanocrystals-Oriented Attachment Mechanism," *CrystEngComm*, **14** [6] 2278–82 (2012).

[16]M. Niederberger and G. Garnweitner, "Organic Reaction Pathways in the Nonaqueous Synthesis of Metal Oxide Nanoparticles," *Chem. Eur. J.*, **12** [28] 7282–302 (2006).

[17]P. H. Mutin and A. Vioux, "Nonhydrolytic Processing of Oxide-Based Materials: Simple Routes to Control Homogeneity, Morphology, and Nanostructure," *Chem. Mater.*, **21** [4] 582–96 (2009).

[18]M. Niederberger, M. H. Bartl, and G. D. Stucky, "Benzyl Alcohol and Titanium Tetrachloride – A Versatile Reaction System for the Nonaqueous and Low-Temperature Preparation of Crystalline and Luminescent Titania Nanoparticles," *Chem. Mater.*, **14** [10] 4364–70 (2002).

[19]R. H. Gonçalves, W. H. Schreiner, and E. R. Leite, "Synthesis of TiO_2 Nanocrystals With a High Affinity for Amine Organic Compounds," *Langmuir*, **26** [14] 11657–62 (2010).

[20]H. Klug and L. Alexander (Eds.), *X-ray Diffraction Procedures: For Polycrystalline and Amorphous Materials*. p.125, Wiley, New York, 1962.

[21]S. Jung, J. Kong, S. Song, K. Lee, T. Lee, H. Hwang, and S. Jeond, "Resistive Switching Characteristics of Solution-Processed Transparent TiO_x for Nonvolatile Memory Application," *J. Electrochem. Soc*., **157** [11] H1042–5 (2010).

[22]G. Valverde-Aguilar, J. A. García-Macedo, V. Renteria-Tapia, and M. Aguilar-Franco, "Photoconductivity Studies of Gold Nanoparticles Supported on Amorphous and Crystalline TiO_2 Matrix Prepared by Sol-Gel Method," *Appl. Phys. A*, **103** [3] 659–63 (2011).

[23]G. Q. Liu, Z. G. Jin, X. X. Liu, T. Wang, and Z. F. Liu, "Anatase TiO_2 Porous Thin Films Prepared by Sol-Gel Method Using CTAB Surfactant," *J. Sol-Gel. Sci. Technol*., **41** [1] 49–55 (2007).

[24]G. L. Li and G. H. Wang, "Morphologies of Rutile Form TiO_2 Twins Crystals," *J. Mater. Sci. Lett*., **18** [15] 1243–6 (1999).

[25]X. Yang, J. Zhuang, X. Li, D. Chen, G. Ouyang, Z. Mao, Y. Han, Z. He, C. Liang, M. Wu, and J. C. Yu, "Hierarchically Nanostructured Rutile Arrays: Acid Vapor Oxidation Growth and Tunable Morphologies," *ACS Nano*, **3** [5] 1212–8 (2009).

[26]M. H. Tsai, S. Y. Chen, and P. Shen, "Imperfect Oriented Attachment: Accretion and Defect Generation of Nanosize Rutile Condensates," *Nano Lett*., **4** [7] 1197–201 (2004).

[27]H. Cheng, J. Ma, Z. Zhao, and L. Qi, "Hydrothermal Preparation of Uniform Nanosize Rutile and Anatase Particles," *Chem. Mater*., **7** [4] 663–71 (1995).

[28]M. P. Finnegan, H. Zhang, and J. F. Banfield, "Phase Stability and Transformation in Titania Nanoparticles in Aqueous Solutions Dominated by Surface Energy," *J. Phys. Chem. C*, **111** [5] 1962–8 (2007).

[29]C. Ribeiro, C. M. Barrado, E. R. de Camargo, E. Longo, and E. R. Leite, "Phase Transformation in Titania Nanocrystals by the Oriented Attachment Mechanism: The Role of the pH Value," *Chem. Eur. J*., **15** [9] 2217–22 (2009).

[30]W. D. Kingery, H. K. Bowen, and D. R. Uhlmann, *Introduction to Ceramics (2nd ed.)*. Chapter 8, Wiley, New York, 1991.

[31]M. R. Mohammadi, D. J. Fray, and A. Mohammadi, "Sol–Gel Nanostructured Titanium Dioxide: Controlling the Crystal Structure, Crystallite Size, Phase Transformation, Packing and Ordering," *Microporous Mesoporous Mater*., **112** [1–3] 392–402 (2008).

[32]H. Mehranpour, M. Askari, and M. S. Ghamsari, "Nucleation and Growth of TiO_2 Nanoparticles"; in *Nanomaterials*, Chap. 2, Edited by M. M. Rahman. InTech, Shangai, China, 2011. http://www.intechopen.com/books/nanomaterials/nucleation-and-growth-of-tio2-nanoparticles. (accessed on December 2011).

[33]L. Liu, H. Liu, Y. P. Zhao, Y. Wang, Y. Duan, G. Gao, M. Ge, and W. Chen, "Diferents Morphology: Directed Synthesis of Hierarchical Nanostructured TiO_2 Catalysts and Their Morphology-Dependent Photocatalysis for Phenol Degradation," *Environ. Sci. Technol*., **42** [7] 2342–8 (2008).

[34]F. Shao, J. Sun, L. Gao, S. Yang, and J. Luo, "Template-Free Synthesis of Hierarchical TiO_2 Structures and Their Application in Dye-Sensitized Solar Cells," *Appl. Mater. Interfaces*, **3** [6] 2148–53 (2011).

[35]V. K. LaMer and R. H. Dinegar, "Theory, Production and Mechanism of Formation of Monodispersed Hydrosols," *J. Am. Chem. Soc*., **72** [11] 4847–54 (1950). □